Journal of Magnetism and Magnetic Materials 324 (2012) 2937–2952

Contents lists available at SciVerse ScienceDirect

Journal of Magnetism and Magnetic Materials

journal homepage: www.elsevier.com/locate/jmmm

Review

Magnetic properties and magnetic structures of the CeScSi-type RMgPb (R=Ce–Nd, Sm, Gd–Tm) compounds

P. Lemoine [a], A. Vernière [a,*], G. Venturini [a], J.F. Marêché [b], S. Capelli [c], B. Malaman [a]

[a] Institut Jean Lamour, dept P2M, équipe 103, CNRS (UMR 7198), Nancy Université B.P. 70239, 54506 Vandoeuvre-les-Nancy Cedex, France
[b] Institut Jean Lamour, dept CP2S, équipe 205, CNRS (UMR 7198), Nancy Université B.P. 70239, 54506 Vandoeuvre-les-Nancy Cedex, France
[c] Institut Laue-Langevin, 38042 Grenoble, France

ARTICLE INFO

Article history:
Received 22 December 2011
Received in revised form
27 February 2012
Available online 9 May 2012

Keywords:
Intermetallic compound
Ternary rare-earth magnesium plumbide
Magnetic property
Neutron powder diffraction
Sine-wave modulated magnetic structure

ABSTRACT

Investigations made by powder X-ray diffraction, magnetic measurements and neutron powder diffraction on the CeScSi-type ternary magnesium plumbides RMgPb (R=Ce–Nd, Sm, Gd–Tm) are reported. Macroscopic magnetic measurements performed in the 2–300 K temperature range show that these compounds follow a Curie–Weiss law in the paramagnetic state (except SmMgPb) and behave antiferromagnetically at low temperature ($T_N \leq 61$ K). Field dependence of the magnetization performed at 5 K evidence metamagnetic-like behaviors ($H_{crit} < 7$ T). Neutron powder diffraction evidenced complex antiferromagnetic structures in fair agreement with the magnetic data. PrMgPb and NdMgPb compounds present a commensurate antiferromagnetic structure, while (Tb–Er)MgPb are characterized by incommensurate sine-wave modulated magnetic structure down to lower temperature or square-wave magnetic structure due to appearance of higher odd integer harmonics. CeMgPb and TmMgPb evidence more complex sine-wave modulated magnetic structures, never encountered with the CeScSi-type structure, characterized by two propagation vectors. These results are discussed and compared with those of the isotypic RMgSn compounds.

1. Introduction

The RMgSn (R=Pr, Nd, Sm, Gd–Tm) compounds crystallize in the CeScSi-type structure [1,2] and exhibit antiferromagnetic behavior below 79 K with metamagnetic-like transitions at low magnetic field ($H_{crit} < 7$ T) [2]. Neutron powder diffraction study evidenced complex magnetic structures which depend of the nature of the rare-earth element. PrMgSn and NdMgSn compounds present a commensurate magnetic arrangement while TbMgSn exhibits a sine-wave modulated magnetic structure from T_N down to the lowest temperature and the RMgSn (R=Dy–Tm) compounds a square-wave modulated magnetic structure at very low temperature due to occurrence of higher order odd integer harmonics [3]. Moreover, it was shown that in this series the magnetic moment orientation of the R atoms is inverse compared to the isotypic compounds [4–6], suggesting an important role of the transition metal on the electrostatic potential in this type structure.

Recently, Provino et al. [7] have reported on the crystal structure of the new ternary RMgPb compounds. They crystallize in CeScSi- (R=Sc, Y, La–Nd, Sm, Gd–Tm, Lu), TiNiSi- (R=Eu, Yb) and ZrNiAl- (R=Yb) types structure.

In order to better understand the magnetism encountered in the CeScSi-type structure compounds, the magnetic properties of the new CeScSi-type RMgPb (R=Ce–Nd, Sm, Gd–Tm) compounds have been studied by macroscopic magnetic measurements and their magnetic structures have been determined by neutron powder diffraction. The results are reported in this paper.

Table 1
Cell parameters at room temperature of RMgPb compounds.

RMgPb	Type-structure	Space group	a (Å)	c (Å)	V (Å^3)	c/a
CeMgPb	CeScSi	I4/mmm	4.557(1)	16.405(1)	340.6(1)	3.60
PrMgPb	CeScSi	I4/mmm	4.532(1)	16.328(1)	335.3(1)	3.60
NdMgPb	CeScSi	I4/mmm	4.510(1)	16.259(1)	330.8(1)	3.61
SmMgPb	CeScSi	I4/mmm	4.471(1)	16.156(1)	322.9(1)	3.61
GdMgPb	CeScSi	I4/mmm	4.444(1)	16.045(1)	316.9(1)	3.61
TbMgPb	CeScSi	I4/mmm	4.423(1)	15.987(1)	312.8(1)	3.61
DyMgPb	CeScSi	I4/mmm	4.407(1)	15.947(1)	309.7(1)	3.62
HoMgPb	CeScSi	I4/mmm	4.395(1)	15.904(1)	307.2(1)	3.62
ErMgPb	CeScSi	I4/mmm	4.382(1)	15.869(1)	304.7(1)	3.62
TmMgPb	CeScSi	I4/mmm	4.369(1)	15.843(1)	302.4(1)	3.63

* Corresponding author. Tel.: +33 0 383684672.
E-mail address: Anne.Verniere@ijl.nancy-universite.fr (A. Vernière).

0304-8853/$ - see front matter © 2012 Elsevier B.V. All rights reserved.
http://dx.doi.org/10.1016/j.jmmm.2012.03.037

2. Experimental methods

The polycrystalline samples were synthesized starting from stoichiometric amounts of high purity (99.9 wt% for lead and rare-earth elements, 99.99 wt% for magnesium metal) commercially available elements. As a general precaution, all sample manipulations were undertaken in a purified argon-filled glove box ensuring an oxygen level of less than 2 ppm O_2 and about 3 ppm H_2O. Owing to the high volatility of magnesium, the elements are placed into an arc-welded Mo crucible. In a first step, the elements were melted in a water-cooled copper crucible using a high frequency induction furnace (CELES), under secondary vacuum. In a second step, to prevent their oxidation, the Mo crucibles were subsequently enclosed in a silica tube under purified argon (300 mm Hg), placed in a furnace for one week at 1073 K and water-cooled. No reaction of the samples with the container material was observed.

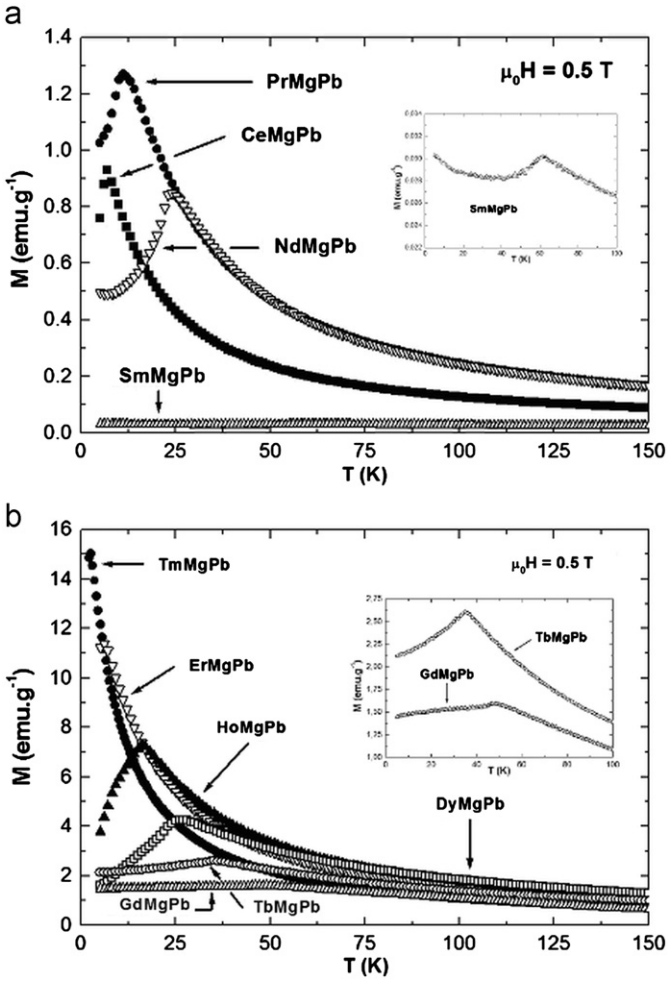

Fig. 1. Thermal variation of the magnetization of CeScSi-type RMgPb (R=Ce, Nd, Sm, Gd – Tm) compounds.

The crystallographic structure and the presence of impurities were checked by powder X-ray diffraction (Philips X'Pert Pro Diffractometer, Cu K_α). The analysis of the patterns was performed by Rietveld profile refinement using the software FULLPROF [8,9]. Profile-matching adjustments were used to refine the cell parameters. It is worth noting that during this stage, it was clearly observed that the samples were not stable in air up to 1 day. Therefore, they were always kept under argon or helium atmosphere.

The magnetic measurements were performed using a conventional PPMS-9 system (Quantum Design) in the 5–300 K (2–300 K for the TmMgPb compound) temperature range and under applied magnetic fields up to 9 T. The thermomagnetic curves were recorded upon heating after zero-field cooling (ZFC). Neutron powder diffraction experiments were carried out at the Institut Laue Langevin (ILL), Grenoble, France. The diffraction patterns were collected with the one-dimensional curved multidetector D1b (λ=2.52 Å) from the paramagnetic state down to ~2 K. In the case of DyMgPb compound, a special double-wall vanadium sample holder was used in order to minimize neutron absorption.

3. Structural data

Ten RMgPb samples have been synthesized and checked with R=Ce, Pr, Nd, Sm, Gd, Tb, Dy, Ho, Er and Tm. The X-ray powder diffraction patterns show unambiguously that these compounds crystallize in the tetragonal CeScSi-type structure (space group *I4/mmm*). In this structure the R, Mg and Pb atoms occupy respectively, the 4(e) [0; 0; z_R~0.34], 4(c) [0; $\frac{1}{2}$; 0] and 4(e) [0; 0; z_{Pb}~0.14]

Table 2
Magnetic data of the CeScSi-type RMgPb and RMgSn compounds.

Compound	T_N (K) (±2 K)	θ_p (K) (±2 K)	m_{eff} (μ_B) (±0.2 μ_B)	M_{max} (μ_B/f.u.) at 5 K for μ_0H=9 T	H_{crit} (T) (±0.2 T)	
CeMgPb	7	20	2.6	1.1	2.8	This work
PrMgPb	11	14	3.7	1.5	2.2	This work
PrMgSn	20	14	3.9	1.9	3.0	[2]
NdMgPb	24	16	3.7	1.0	6.2	This work
NdMgSn	31	2	4.0	1.3	6.0	[2]
SmMgPb	61	–	–	0.02	–	This work
SmMgSn	79	–	–	0.02	–	[2]
GdMgPb	47	−3	7.9	1.3	–	This work
GdMgSn	48	−16	8.2	1.6	7.0	[2]
TbMgPb	35	−11	10.0	3.7	7.0	This work
TbMgSn	34	−11	10.2	4.4	6.4	[2]
DyMgPb	26	−10	11.4	7.2	2.6	This work
DyMgSn	27	−6	11.4	7.5	2.6	[2]
HoMgPb	16	0	10.7	8.9	2.0	This work
HoMgSn	17	−2	10.9	8.9	1.8	[2]
ErMgPb	6	7	9.6	7.2	1.6	This work
ErMgSn	8	7	9.8	7.2	1.4	[2]
TmMgPb	2.5	19	7.7	5.6	–	This work
TmMgSn	3	20	7.7	5.8	–	[3], This work

crystallographic sites. The cell parameters refined at room temperature are gathered in Table 1. One of the remarkable features is the great stability of the CeScSi-type structure in the RMgPb series. According to Provino et al. [7] and the present data, one can conclude that the RMgPb series is the first example of CeScSi-type ternary compounds stable for all the R^{3+} rare-earth elements.

4. Magnetic measurements

The thermal variations of the magnetization are displayed in Fig. 1. For all the RMgPb compounds (R=Ce, Pr, Nd, Sm, Gd, Tb, Dy, Ho, Er and Tm), the magnetic curves exhibit a typical shape of antiferromagnetic behavior with Néel temperatures ranging between 2.5 and 61 K (Fig. 1 and Table 2). The ordering temperature obtained experimentally are compared in Fig. 2 with those predict by the de Gennes law [10]. For the heavy rare-earth compounds (Gd–Tm), the Néel temperatures well obey the de Gennes rule. It means that their magnetic properties may be considered in terms of R.K.K.Y. model of indirect exchange interactions between the *4f* moments via conduction electron [11–13]. By contrast, the magnetic temperature ordering of light rare-earth compounds are significantly higher than the de Gennes factor. Similar behavior has been already observed in RMgSn CeScSi-type compounds [2] and in the ternary equiatomic RAuSn LiGaGe- [14], RTiGe CeFeSi- [15] and RRhZn TiNiSi-type compounds [16]. The origin of these anomalies should probably not be explained by crystal electric field effect alone and should be due to strong *4f*-conduction electrons interactions [17].

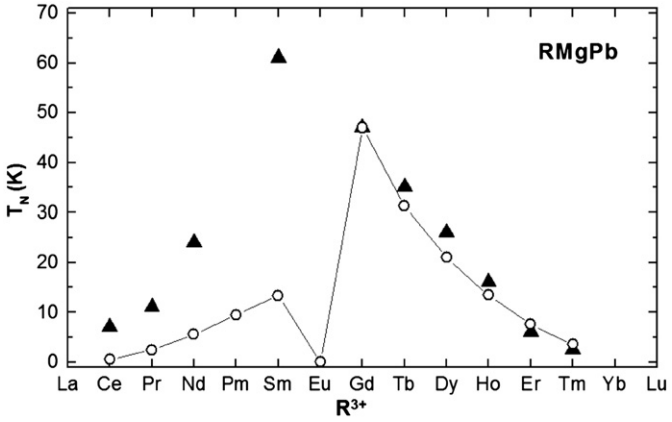

Fig. 2. Observed Néel temperatures in the CeScSi-type RMgPb compounds (▲) and their relation to the de Gennes function (○, normalized to R=Gd).

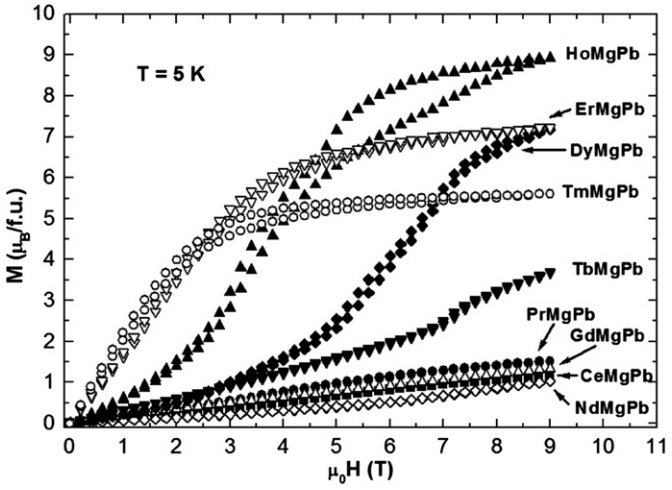

Fig. 3. Field dependence of the magnetization at 5 K of CeScSi-type RMgPb compounds.

In the paramagnetic range, thermal dependence of the magnetic susceptibility has been fitted by the Curie–Weiss law, excepted for the SmMgPb compound, suggesting a Van Vleck contribution of the Sm ions. The experimental effective values of the R moments given in Table 2 are in good agreement with the R^{3+} free ion values. The paramagnetic Curie temperatures (θ_p) are close to zero (slightly positives for the Ce, Pr, Nd, Er and Tm compounds, Table 2) and suggested non-negligible ferromagnetic interactions in these compounds.

The field dependence of the magnetization at 5 K recorded in fields up to 9 T is shown in Fig. 3. These curves exhibit a linear part at low magnetic field and display a metamagnetic-like transition without magnetic remanence in agreement with the antiferromagnetic behavior detected on the thermomagnetic curves. Only HoMgPb curve clearly shows rather large magnetic hysteresis at high field. The curves of GdMgPb and TmMgPb compounds do not exhibit metamagnetic-like transition up to 9 T. According to the evolution of the critical fields, this transition would probably appear at higher magnetic field for GdMgPb. For TmMgPb, the magnetization curve is not therefore in contradiction with an antiferromagnetic order in so far as the magnetic order appears just a few Kelvin (T_N=2.5 K) below the temperature of measurements. The weak threshold field values suggest the existence of rather weak antiferromagnetic interactions. In all cases, the maximum values of the magnetization are lower than the theoretical free ions values (Table 2) in fair agreement with absence of magnetization saturation at μ_0H=9 T (Fig. 3).

5. Neutron diffraction measurements

Neutron thermograms and long duration patterns at ~2 K and in the paramagnetic state were recorded for the RMgPb (R=Ce–Nd, Tb–Tm) compounds. The powder neutron diffraction patterns recorded in the paramagnetic state confirm the CeScSi-type structure. The results of refinements performed in the paramagnetic state are gathered in Table 3. The crystallographic cell of the CeScSi-type structure is characterized by four rare-earth atoms at the positions: (0, 0, z_R), ($\frac{1}{2}$, $\frac{1}{2}$, $\frac{1}{2}+z_R$), (0, 0, $-z_R$) and ($\frac{1}{2}$, $\frac{1}{2}$, $\frac{1}{2}-z_R$). These atoms are connected two by two by the body-centered Bravais lattice (Fig. 4).

Table 3
Refined parameters of RMgPb (R=Ce–Nd, Tb–Tm) compounds in the paramagnetic state.

	CeMgPb	PrMgPb	NdMgPb	TbMgPb	DyMgPb	HoMgPb	ErMgPb	TmMgPb
	15 K	20 K	30 K	50 K	35 K	25 K	15 K	8 K
a (Å)	4.539(2)	4.513(1)	4.495(1)	4.405(1)	4.395(2)	4.379(2)	4.367(1)	4.347(2)
c (Å)	16.342(7)	16.267(4)	16.193(3)	15.930(4)	15.915(5)	15.846(5)	15.811(5)	15.828(5)
z_R	0.330(1)	0.335(1)	0.335(1)	0.333(1)	0.334(1)	0.334(1)	0.334(1)	0.333(1)
z_{Pb}	0.134(1)	0.135(1)	0.135(1)	0.138(1)	0.137(1)	0.139(1)	0.139(1)	0.139(1)
R_{Bragg}; R_f	7.07; 4.54	3.06; 2.27	2.11; 1.87	1.84; 1.90	4.47; 2.60	5.17; 4.50	3.43; 3.27	6.61; 4.47
R_{wp}; R_{exp}; χ^2	5.83; 0.57; 104	2.76; 0.74; 13.8	2.29; 0.83; 7.60	2.07; 0.46; 20.0	0.854; 0.47; 3.33	2.38; 0.61; 15.3	1.89; 0.83; 5.20	2.24; 0.82; 7.49

The refinements were performed in the "spherical coordinates procedure" of the Fullprof software [8]. The three extra parameters characterizing the atomic magnetic moments correspond to the value of μ_R (in Bohr magnetons), the spherical θ angle with the z axis and the spherical ϕ angle with the x axis. In this mode, the z axis is along c while the x axis is aligned along a (i.e. axis of the unit cell).

Remark: Diffraction peaks of low intensity, corresponding to a wavelength $\lambda/2$, are observed on the neutron diffraction patterns. These peaks are distinguished by the symbol $*$ and excluded from the refinement.

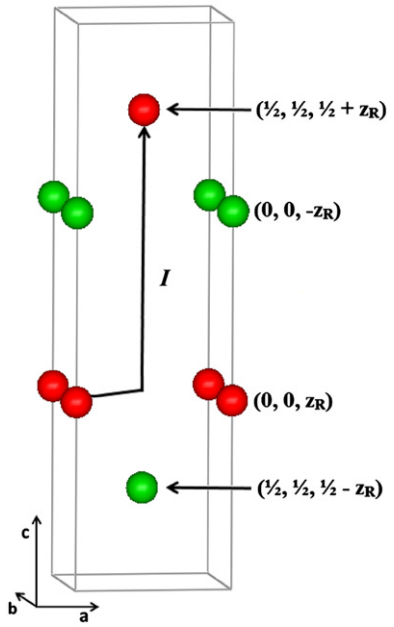

Fig. 4. Representation of the two R "sublattices" in the CeScSi-type structure.

5.1. Neutron diffraction study of CeMgPb

The pattern recorded at 2 K (Fig. 5), displays additional magnetic peaks which can be indexed considering two propagation vectors, one commensurate $k_1 = [\frac{1}{2}, \frac{1}{2}, 0]$, and a second incommensurate $k_2 = [0.448, \frac{1}{2}, 0]$. The presence of magnetic reflections obeying the rule $h+k+l=2n+1$ indicates an anti-I mode, while extinction of those with $l=3n$ allow to exclude "$+--+$" sequence of magnetic moment along the [001] direction due to the

Table 4
Refined parameters of CeMgPb compound at 2 K.

a (Å)	4.538(1)
c (Å)	16.339(4)
z_{Ce}	0.330(1)
z_{Pb}	0.134(1)
Antiferromagnetic	
θ (deg.)	90
ϕ (deg.)	135
propagation vector k_1	[0.5; 0.5; 0]
μ_{Ce} (μ_B)	1.38(5)
Sine-modulated	
$A(k)_{Ce}$	1.23(11)
θ (deg.); ϕ (deg.)	90; 135
propagation vector k_2	[0.448(3); 0.5; 0]
μ_{Ce}[a] (μ_B)	0.87
$\mu_{Ce\ total}$ (μ_B)	2.25
R_{Bragg}; R_f	4.25; 3.17
R_{magn}	20.0; 26.5
R_{wp}; R_{exp}; χ^2	3.59; 0.55; 41.7

[a] The mean magnetic moment in a sine-modulated structure μ_i is calculated from the amplitude $A(k)_i$ with the relation $\mu = A(k)2^{-1/2}$.

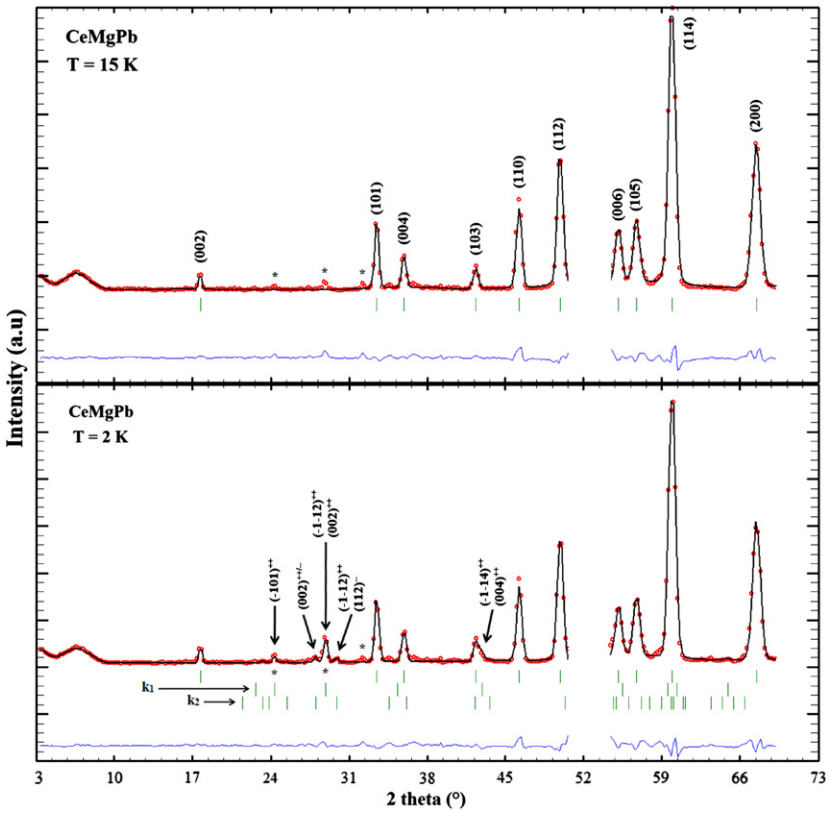

Fig. 5. Observed and calculated neutron diffraction patterns of CeMgPb at 15 and 2 K.

cancellation of the structure factor in relation to the particular z coordinate of the R atoms ($z_R \sim 1/3$) [3]. Thus, the right sequence is "++−−", inducing opposite magnetic moments for the (0, 0, z_R) and (0, 0, $-z_R$) atoms (cf. Fig. 4). The low intensity of magnetic peaks, and the presence of nuclear contribution, coming from $\lambda/2$ wavelength, under the $(-101)^{++}$, $(-1-12)^{++}$ and $(002)^{++}$ magnetic reflections (Fig. 5) make difficult the refinement of orientation and intensity of magnetic moments. For these two phases, the best refinement is obtained considering magnetic moments lying in the (a,b) plan with a ϕ angle of 135°. For the magnetic phase corresponding to the propagation vector k_2, the best result is obtained with a sine-wave modulated magnetic structure with respect to a helimagnetic structure. The final refinements lead to a magnetic moment values of 1.38(5) μ_B/Ce for the first magnetic phase and amplitude of 1.23(11) μ_B/Ce (corresponding to a mean magnetic moment of 0.87 μ_B/Ce calculated from the amplitude $A(k)$ with the relation $\mu = A(k)2^{-1/2}$) for the second magnetic phase (Table 4). Neutron thermogram evidenced a simultaneously increasing of the magnetic reflections of the two propagation vectors below 6 K without thermal evolution. Due to the weak

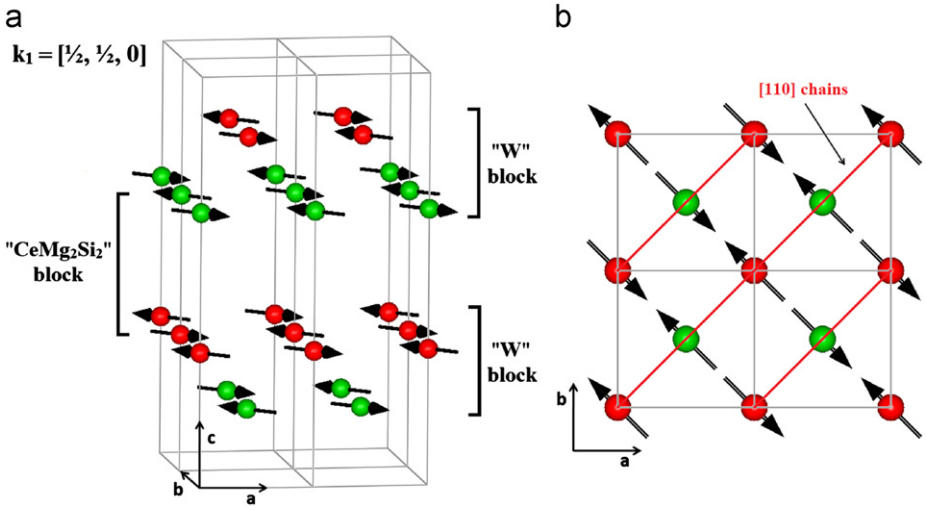

Fig. 6. Magnetic structure corresponding to the propagation vector k_1 of CeMgPb.

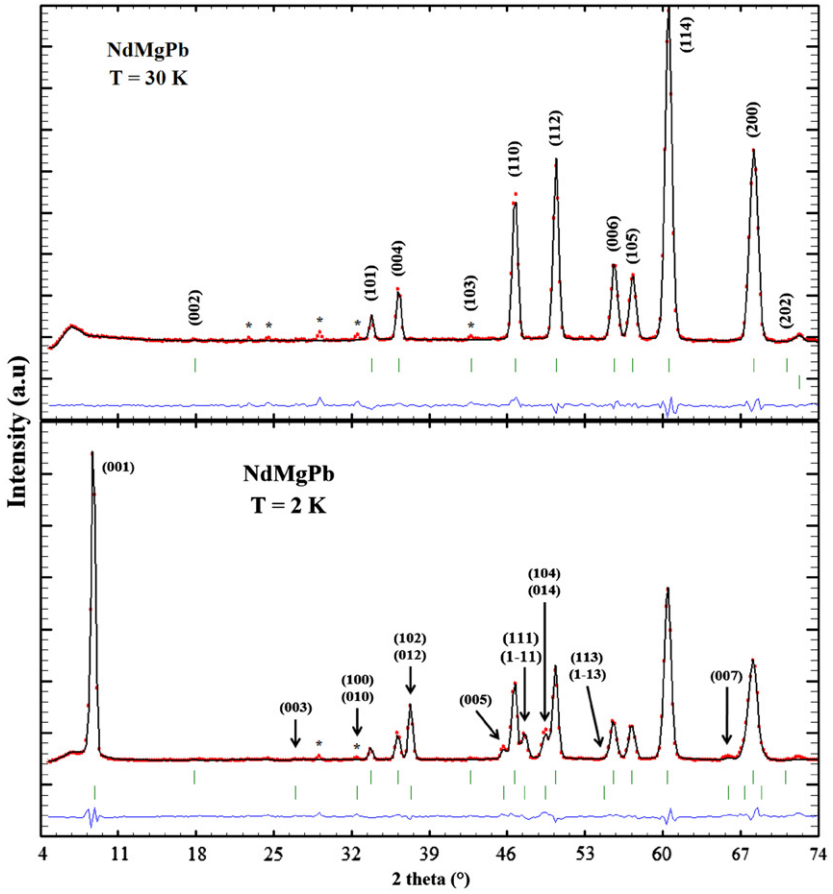

Fig. 7. Observed and calculated neutron diffraction patterns of NdMgPb at 30 and 2 K.

intensity and the low ordering temperature, no higher order harmonics are evidenced for the second magnetic phase.

The magnetic structure of the commensurate phase (phase "1"), shown on Fig. 6, is characterized by ferromagnetic [110] chains coupling antiferromagnetically between them within the "W" blocks (Fig. 6(b)). These blocks are coupled antiferromagnetically between first neighbors in the [001] direction ("$CeMg_2Si_2$" blocks, Fig. 6(a)). The magnetic structure of the incommensurate phase (phase "2") is similar taking into account the modulation of the magnetic moments in the [100] direction.

5.2. Neutron diffraction study of PrMgPb and NdMgPb

The patterns recorded in the magnetic state for these two compounds display additional peaks (as shown in the Fig. 7 for the NdMgPb compound), which can be indexed with a commensurate propagation vector $k=[1, 0, 0]$ or $[0, 0, 1]$. According to Rossat-Mignod [18], for a c parameter greater than a parameter, the right propagation vector is $k=[0, 0, 1]$.

Below 14 K and 26 K for PrMgPb and NdMgPb, respectively, the increase of the (hkl) reflections with $h+k+l=2n+1$, and the extinction of those with $l=3n$ indicate an opposite magnetic moments for the $(0, 0, z_R)$ and the $(0, 0, -z_R)$ atoms ($z_R \sim 1/3$), and lead to the "++− −" sequence along the [001] direction. Magnetic contribution to the (001) and (005) reflections indicate a deviation of the magnetic moment from the c axis. At 2 K, the best refinements are obtained considering a deviation of the magnetic moment from the (a,b) plane. The refined θ angle is close to 58(2)° and 57(1)° for PrMgPb and NdMgPb, respectively (Table 5). The magnetic structure at 2 K, shown in Fig. 8, evidences ferromagnetic coupling in the "W" blocks and antiferromagnetic in the "$CeMg_2Si_2$" blocks.

Refinements of the patterns recorded between T_N and 2 K evidence a saturation of the magnetic moments of $\sim 1.80\ \mu_B$ and $\sim 3.38\ \mu_B$ for PrMgPb and NdMgPb, respectively (Fig. 9). The refined Nd moment value is close to the Nd^{3+} free ion ($3.27\ \mu_B$), while the refined Pr moment value is smaller than that expected for the Pr^{3+} free ion ($3.20\ \mu_B$), indicating a probable crystal electric field effect for this compound [19,20]. No thermal evolution of the magnetic structure is observed.

5.3. Neutron diffraction study of TbMgPb, DyMgPb, HoMgPb and ErMgPb

5.3.1. TbMgPb compound

The diffraction pattern recorded at 2 K, evidences additional magnetic peaks (Fig. 10) which can be indexed with a propagation vector $k=[0.843, 0, 0]$, indicating an incommensurate antiferromagnetic structure. The refinement has been undertaken with a sine-wave modulated structure. Absence of higher order harmonics allow to exclude a possible square-wave magnetic structure. Extinction of the (hkl) reflections with $l=3n$ indicates an opposite magnetic phase

Table 5
Refined parameters of PrMgPb and NdMgPb compounds at 2 K.

	PrMgPb	NdMgPb
a (Å)	4.514(1)	4.500(1)
c (Å)	16.272(3)	16.217(3)
z_R	0.335(1)	0.335(1)
z_{Pb}	0.134(1)	0.135(1)
Antiferromagnetic		
θ (deg.)	58(2)	57(1)
μ_R (μ_B)	1.80(3)	3.38(4)
R_{Bragg}; R_f	3.01; 2.38	4.37; 2.98
R_{magn}	4.36	4.94
R_{wp}; R_{exp}; χ^2	2.99; 0.73; 16.7	3.57; 0.69; 26.9

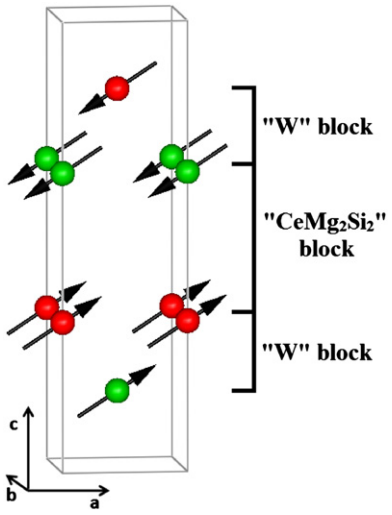

Fig. 8. Magnetic structure of PrMgPb and NdMgPb compounds.

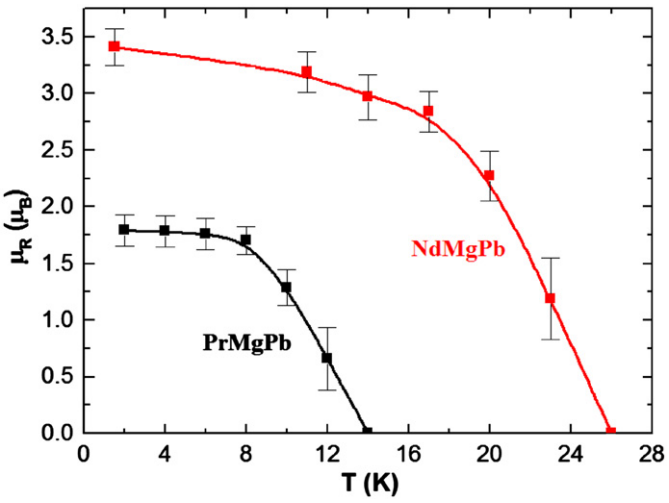

Fig. 9. Thermal variation of the magnetic moment of PrMgPb and NdMgPb.

angle for the $(0, 0, z_R)$ and the $(0, 0, -z_R)$ atoms ($z_R \sim 1/3$). The best refinement is obtained with the Tb magnetic moments oriented in the (a,b) plane ($\theta=90°$, $\phi=42°$) and a magnetic amplitude $A(k)$ of the sine-wave of 11.47(10) μ_B (Table 6), corresponding at a mean magnetic moment $\mu_{Tb}=8.11\ \mu_B$, calculated from the amplitude $A(k)_i$ with the relation $\mu=A(k)2^{-1/2}$. This value is slightly smaller than those expected for the Tb^{3+} free ion ($gJ\mu_B=9.00\ \mu_B$). The q_x component, rather close to 5/6 (~ 0.833), allows to represent in first approximation the sine-wave modulated structure in a magnetic cell six-times larger along the [100] direction than the chemical one (Fig. 11(a)). The Tb magnetic moments are modulated in the [100] and [010] directions due to the ϕ angle of 42°.

The neutron thermogram evidences a slightly thermal variation of the q_x component of the propagation vector. Its value increases from 0.827 to 0.843 between T_N and 16 K, and remains constant down to 2 K. A thermal evolution of the ϕ angle is also observed from 29° to 42° in the same temperature range (Fig. 12). The thermal variation of the magnetic moment (Fig. 13) evidences a magnetic ordering below 39 K.

5.3.2. DyMgPb compound

At 2 K, the neutron diffraction pattern evidences some additional magnetic peaks (Fig. 14), which can be indexed with a

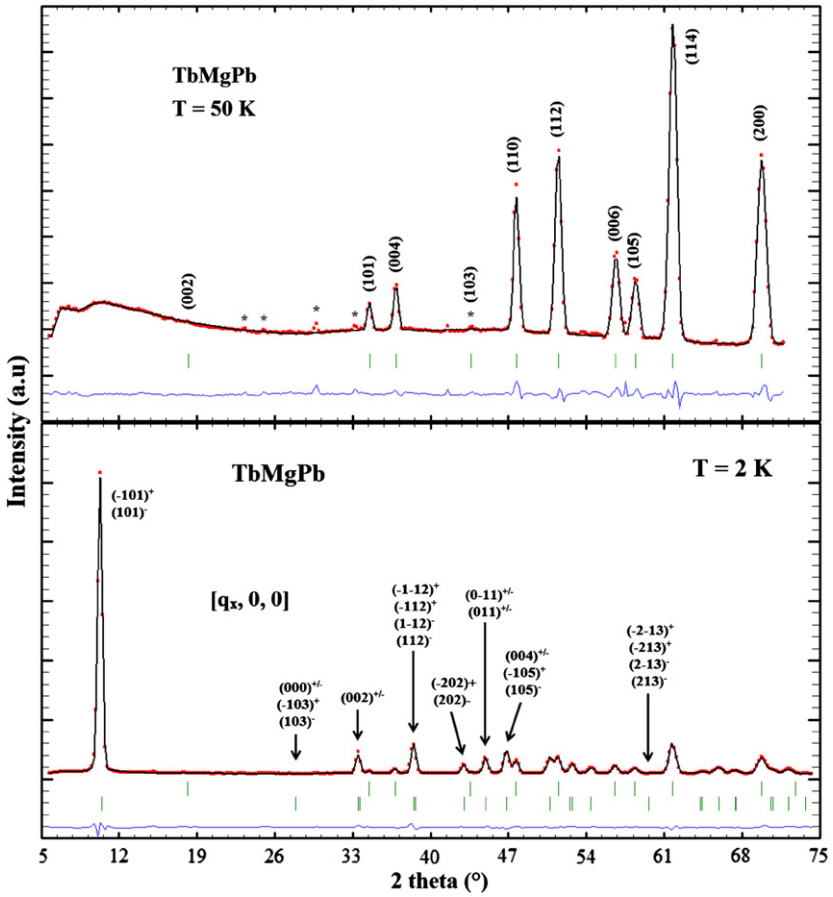

Fig. 10. Observed and calculated neutron diffraction patterns of TbMgPb at 50 and 2 K.

Table 6
Refined parameters of TbMgPb, DyMgPb, HoMgPb and ErMgPb compounds in the magnetic state.

	TbMgPb	DyMgPb	HoMgPb		ErMgPb	
	2 K	2 K	13 K	2 K	5 K	2 K
a (Å)	4.407(1)	4.397(1)	4.384(1)	4.383(1)	4.368(1)	4.364(1)
c (Å)	15.948(3)	15.923(5)	15.861(3)	15.856(4)	15.818(3)	15.801(3)
z_R	0.334(1)	0.335(1)	0.334(1)	0.334(1)	0.334(1)	0.334(1)
z_{Pb}	0.137(1)	0.140(2)	0.139(1)	0.139(2)	0.139(1)	0.139(1)
Sine-modulated						
θ (deg.)	90	90	90	90	0	0
ϕ (deg.)	42(1)	138(2)	71(1)	47(2)	0	0
$A(k)_R$	11.47(10)	10.34(11)	7.72(7)	12.17(12)	6.47(5)	9.69(6)
q_x	0.843(1)	0.841(1)	0.829(1)	0.835(1)	0.813(1)	0.816(1)
q_y	0	0.016(1)	0	0	0	0
μ_R[a] (μ_B)	8.11	7.31	5.46	8.61	4.58	6.85
Third harmonic						
$A(3k)_R$	–	2.56(11)	–	3.99(11)	–	2.74(7)
$3q_x$	–	0.524(1)	–	0.506(1)	–	0.448(1)
$3q_y$	–	0.047(1)	–	0	–	0
μ_R[a] (μ_B)	–	1.81	–	2.82	–	1.94
Fifth harmonic						
$A(5k)$ R	-	1.47(11)	–	2.50(14)	–	–
$5q_x$	–	0.206(1)	–	0.177(1)	–	–
$5q_y$	–	0.079(1)	–	0	–	–
μ_R[a] (μ_B)	–	1.04	–	1.77	–	–
$\mu_{R\ total}$ (μ_B)	8.11[a]	8.12[b]	5.46[a]	9.56[b]	4.58[a]	7.61[b]
R_{Bragg}; R_f	5.81; 4.50	4.22; 2.82	3.57; 2.12	5.97; 4.33	4.27; 3.05	4.08; 2.68
R_{magn}	3.19; -; -	7.17; 22.9; 55.5	5.93; -; -	2.71; 35.3; 52.0	8.44; -; -	4.19; 27.8; -
R_{wp}; R_{exp}; χ^2	5.31; 0.52; 103	1.35; 0.24; 30.9	3.41; 0.54; 39.6	6.41; 0.46; 193	2.60; 0.80; 10.5	2.98; 0.71; 17.7

[a] The mean magnetic moment in the sine-modulated structure μ_i is calculated from the amplitude $A(k)_i$ with the relation $\mu = A(k)2^{-1/2}$.
[b] The mean magnetic moment in the square-modulated structure μ is calculated from the amplitudes $A(k)$ of the fundamental sine-wave with the relation $\mu = A(k)\pi/4$.

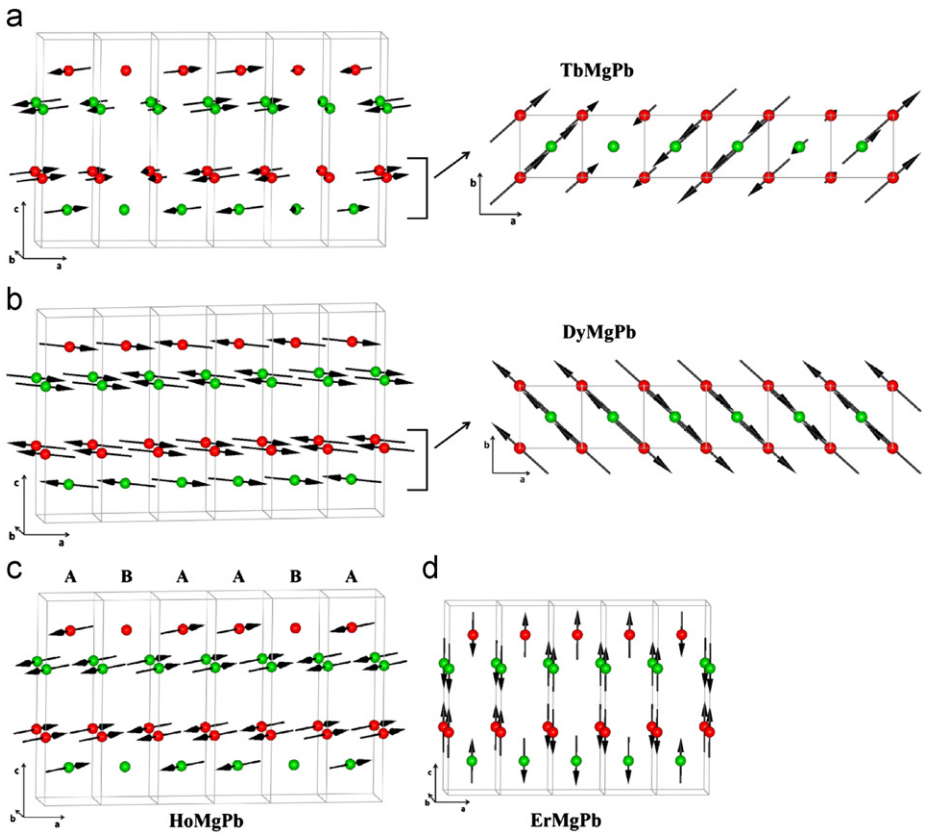

Fig. 11. Magnetic structures of TbMgPb (a), DyMgPb (b), HoMgPb (c) and ErMgPb (d) compounds at 2 K.

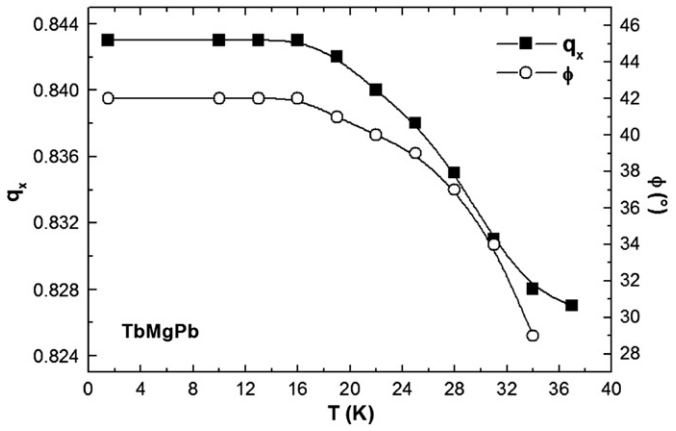

Fig. 12. Thermal variation of the q_x component and ϕ angle of TbMgPb.

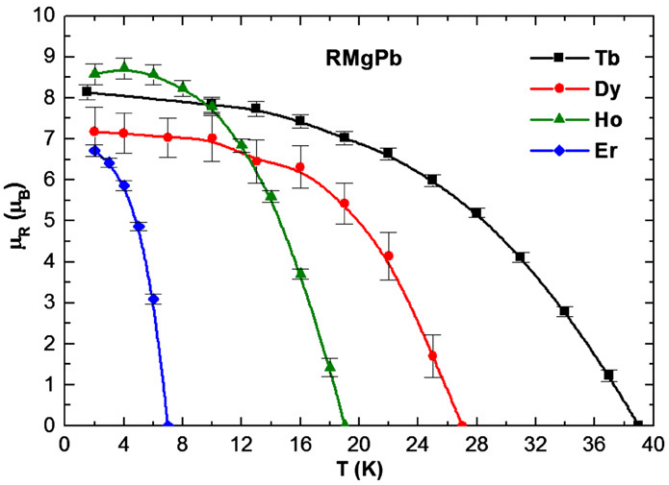

Fig. 13. Thermal variation of the magnetic moment of the (Tb–Er)MgPb compounds.

propagation vector close to that obtained for the TbMgPb compound. However, the splitting of the (hkl) peaks with $k \neq 0$, involves the existence of a q_y component, yielding the propagation vector $k_1=[0.841, 0.016, 0]$. Other smaller supplementary magnetic reflections observed at 2 K (Fig. 14) can be indexed considering a second propagation vector $k_2=[0.524, 0.047, 0]$ and a third propagation vector $k_3=[0.206, 0.079, 0]$ corresponding to the third and the fifth order harmonics, respectively. Presence of higher order harmonics is difficult to determine unambiguously due to the important absorption of dysprosium and the very weak amplitude of involved peaks. Indeed, the relative values of the amplitude of harmonics k_i decrease according to the relation $A(k_i)=A(k_1)/i$ $(i=3, 5, 7, \ldots)$ [21]. However, observation of the second and third odd integer harmonics suggest an incommensurate square-wave magnetic structure at lower temperature.

Extinction of the $(hkl)^{\pm}$ satellites with $l=3n$ corresponds to an opposite magnetic phase angle for the $(0, 0, z_R)$ and $(0, 0, -z_R)$ atoms ($z_R \sim 1/3$). The best refinement at 2 K is obtained with the Dy magnetic moments oriented in the (a,b) plane, a ϕ angle close to 138° and magnetic amplitudes of 10.34(11), 2.56(11) and 1.47(11) μ_B for the fundamental sine-wave, the third and the fifth harmonics, respectively (Table 6). For a square-wave magnetic structure, the mean magnetic moment μ is calculated from the amplitude $A(k)$ of the fundamental sine-wave with the relation

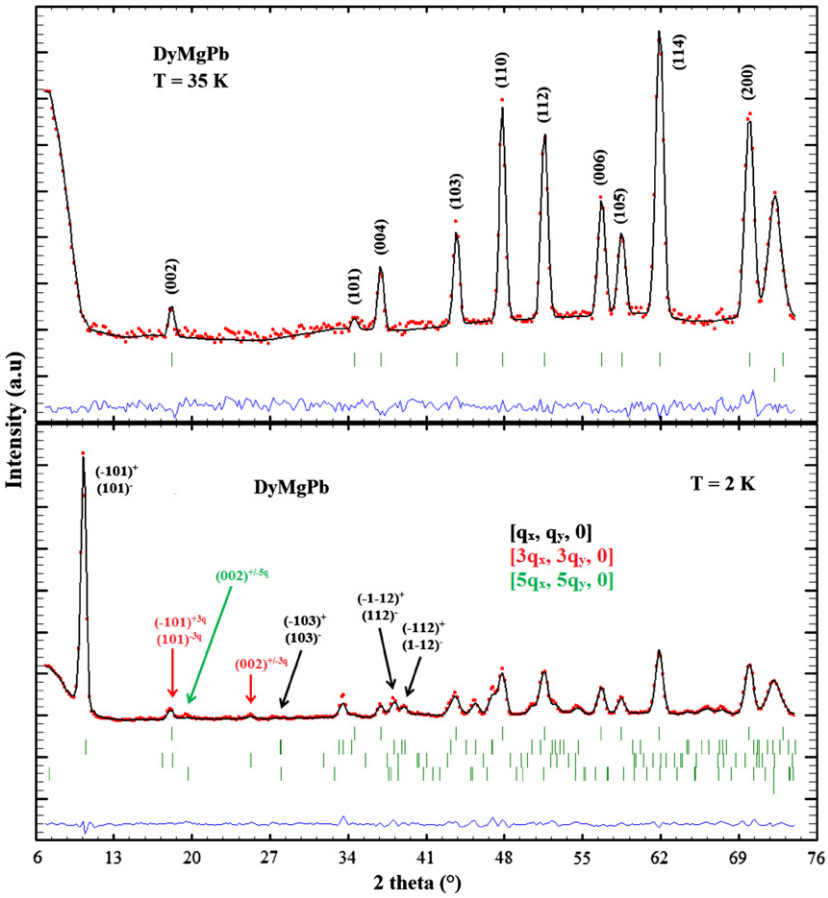

Fig. 14. Observed and calculated neutron diffraction patterns of DyMgPb at 35 and 2 K.

$\mu = A(k)\pi/4$. Thus, the mean magnetic moment of dysprosium is 8.12(11) μ_B at 2 K (Table 6). This value is slightly weak compared with those expected for the Dy^{3+} free ion ($gJ\mu_B = 10.00\ \mu_B$).

The thermal variation of the magnetic moment evidences a magnetic ordering below 27 K (Fig. 13). The Dy magnetic moments amplitude is modulated in the [100] and [010] directions ($\phi \sim 138^\circ$, Fig. 11(b)) with a wavelength close to six crystallographic cells in the [100] direction ($q_x \sim 5/6$). Due to the q_y component of 0.016(1), supplementary modulation exists in the [010] direction with a wavelength of ~60–70 crystallographic cells.

5.3.3. HoMgPb compound

The additional magnetic peaks at 2 K (Fig. 15) can be indexed by the propagation vector $k_1 = [0.835, 0, 0]$, indicating an antiferromagnetic order. At this temperature, the value of the q_x component, very close to 5/6, suggested a commensurate magnetic structure. A square-wave magnetic structure is assumed at very low temperature in relation with the existence of the higher order harmonics $k_2 = [3q_x, 0, 0]$ and $k_3 = [5q_x, 0, 0]$. Extinction of the $(hkl)^{\pm}$ satellites with $l = 3n$ indicates an opposite magnetic phase angle for the $(0, 0, z_R)$ and $(0, 0, -z_R)$ atoms ($z_R \sim 1/3$). The best refinement is obtained with the Ho magnetic moment oriented in the (a,b) plane ($\theta = 90^\circ$, $\phi \sim 47^\circ$) and magnetic amplitudes of 12.17(12), 3.99(11) and 2.50(14) μ_B for the fundamental sine-wave, the third and the fifth harmonics, respectively (Table 6). The mean magnetic moment calculated with the relation $\mu = A(k)\pi/4$ (square-wave magnetic structure) is 9.56 μ_B at 2 K. This value is close to that of the Ho^{3+} free ion ($gJ\mu_B = 10.00\ \mu_B$). The Ho magnetic moments are modulated in the [100] and [010] directions ($\phi \sim 47^\circ$) with a wavelength corresponding to six crystallographic cells in the [100] direction ($q_x = 5/6$). Thus, the magnetic structure can be described by the units A and B, which correspond to one crystallographic cell, with the sequence ABAABA (Fig. 11(c)). In these units, the magnetic couplings between holmium atoms localized in the (0, 0, 0.334) and (0, 0, 0.666) positions ("$CeMg_2Si_2$" block) are antiferromagnetic, while the magnetic couplings between holmium atoms in the (0, 0, 0.334) and ($\frac{1}{2}$, $\frac{1}{2}$, 0.166) positions ("W" block) are ferromagnetic in the unit A and both ferromagnetic and antiferromagnetic in the unit B, inducing a magnetic frustration of the holmium atoms in the ($\frac{1}{2}$, $\frac{1}{2}$, 0.166) position (Fig. 11(c)).

The thermal variation of the magnetic moment (Fig. 13) evidences a magnetic ordering below 19 K with a pure sine-wave modulated magnetic structure, supported by the long duration pattern recorded at 13 K (Fig. 15 and Table 6). Below 10 and 6 K, neutron thermograms show the apparition of the higher order harmonics $3q_x$ and $5q_x$, respectively (Fig. 16(a)). The value of the q_x component increases from 0.820 to 0.835 between 18 and 10 K and remains constant down to 2 K. A thermal evolution of the ϕ angle is fitted from 77° to 48° between 16 and 6 K and remains constant down to 2 K (Fig. 16(b)).

5.3.4. ErMgPb compound

The neutron diffraction pattern recorded at 2 K exhibits some magnetic peaks indexed with a propagation vector $k_1 = [0.816, 0, 0]$ (Fig. 17). Existence of higher order harmonic $k_2 = [3q_x, 0, 0]$ suggest a square-wave magnetic structure at lower temperature. Extinction of the $(hkl)^{\pm}$ satellites with $l = 3n$ indicates an opposite magnetic

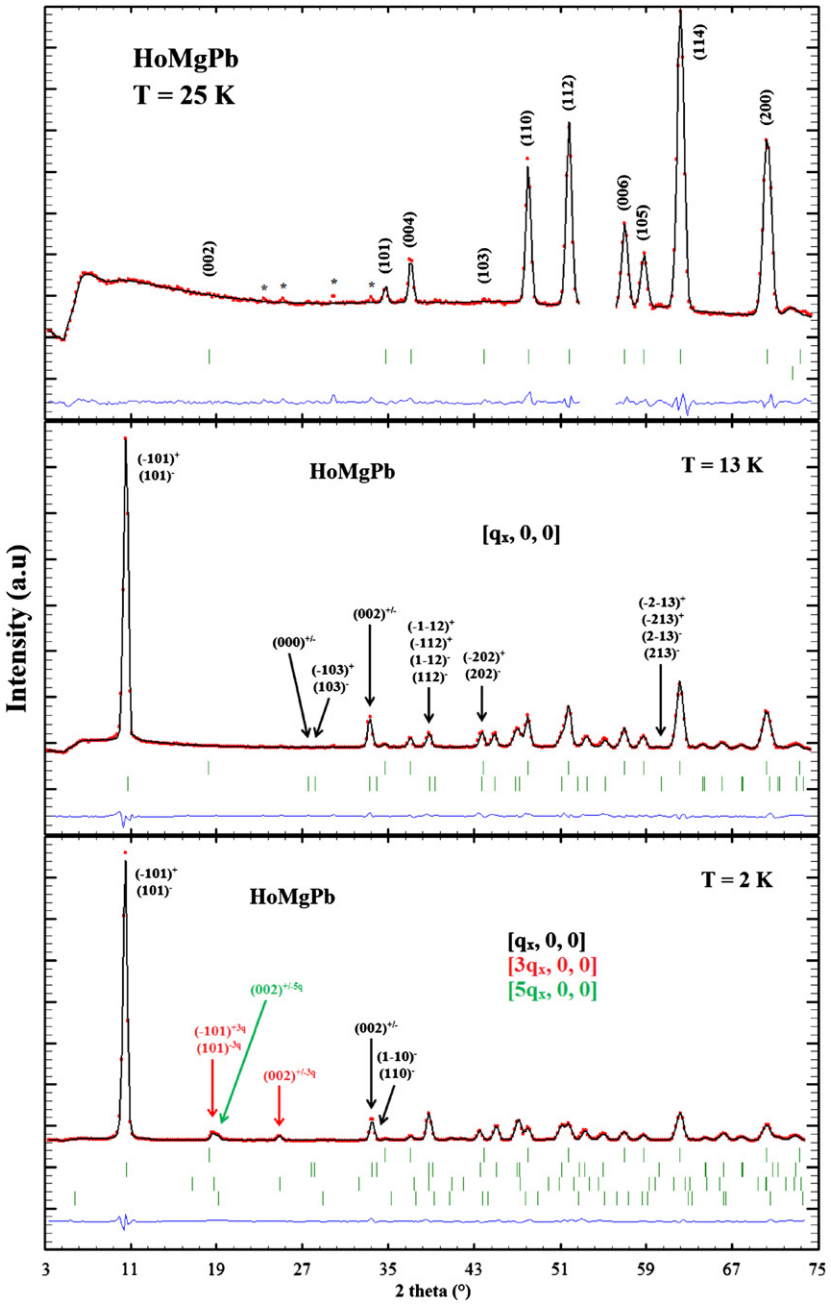

Fig. 15. Observed and calculated neutron diffraction patterns of HoMgPb at 25, 13 and 2 K.

phase angle for the (0, 0, z_R) and (0, 0, $-z_R$) atoms ($z_R \sim 1/3$). Refinement indicates an alignment of the magnetic moments along the c axis ($\theta = 0^\circ$) with magnetic amplitudes of 9.69(6) and 2.74(7) μ_B for the fundamental sine-wave and the third harmonic, respectively (Table 6). It is impossible to observe unambiguously the fifth order harmonic due to the localization of magnetic reflections under other diffraction peaks. The mean magnetic moment calculated with the relation $\mu = A(k)\pi/4$ (square-wave magnetic structure) is 7.61 μ_B at 2 K. This value is weaker than that expected for Er^{3+} free ion ($gJ\mu_B = 9.00\ \mu_B$). The thermal variation of the magnetic moments (Fig. 13) evidences a magnetic ordering below 7 K and neutron diffraction patterns recorded step by step show the appearance of the first odd integer harmonic below 4 K (Fig. 18), supported by the long duration pattern recorded at 5 K (Fig. 17 and Table 6).

The q_x component, rather close to 4/5 ($\sim$0.800), allows to represent in first approximation the square-wave magnetic structure in a magnetic cell five-times larger along the [100] direction than the chemical one (Fig. 11(d)). The Er magnetic moments are modulated only in the [100] direction due to the θ angle of 0°.

5.4. Neutron diffraction study of TmMgPb

The neutron diffraction patterns recorded at 2 and 1.4 K evidenced supplementary magnetic peaks (Fig. 19). At 1.4 K, these peaks can be indexed with two propagation vectors $k_1 = [0.412, 0, 0]$ and $k_2 = [0.447, 0, 0]$. At 2 K, intensities of the magnetic peaks corresponding to the propagation vector k_2 are very weak, while those of the propagation vector k_1 are broad thus suggesting the

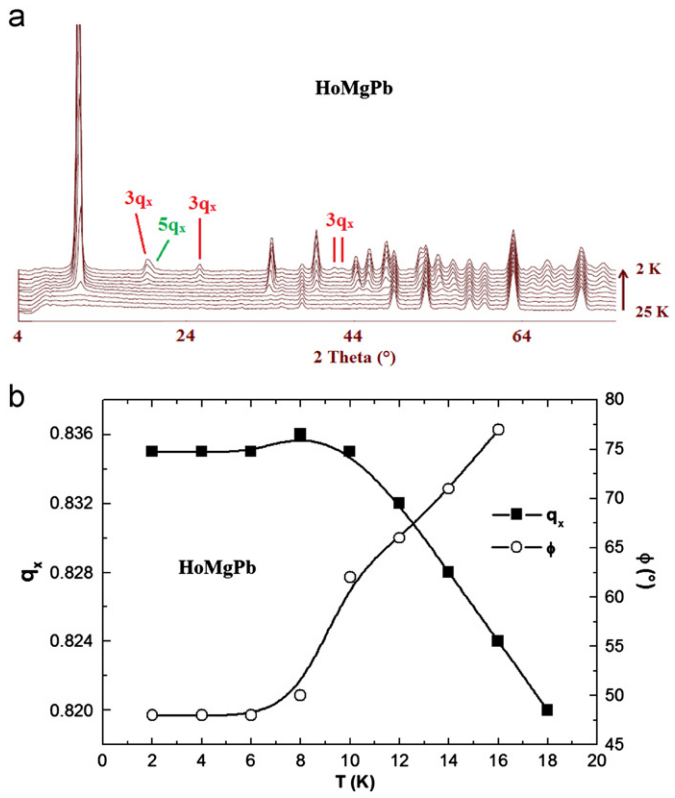

Fig. 16. Neutron thermogram (a) and thermal variation of the q_x component and ϕ angle (b) of HoMgPb.

contribution of a q_z component (Table 7). These results confirm the antiferromagnetic ordering of this compound at very low temperature and suggest an incommensurate magnetic structure with thermal evolution. The observation of the $(hkl)^{\pm}$ satellites with $l=3n$ indicates that the (0, 0, z_R) and (0, 0, $-z_R$) atoms ($z_R \sim 1/3$) do not present an opposite magnetic phase angle. The best refinements at 2 and 1.4 K are obtained with sine-wave modulated magnetic structures and lead to a magnetic moments orientation along the c axis ($\theta=0^\circ$). The phase angle close to 0° indicates same sign and amplitude for the magnetic moment of the (0, 0, z_R) and (0, 0, $-z_R$) atoms (Table 7). Absence of higher order harmonics suggests a pure sine-wave modulated structure. However, the low ordering temperature does not allow to exclude appearance of them below 1.4 K and a square-wave magnetic structure at 0 K. The magnetic structure corresponding to the propagation vector k_1 is shown on Fig. 20. Due to θ angle of 0°, these magnetic structures evidenced only a modulation in the [100] direction. Amplitudes of the k_1 and k_2 propagation vectors, at 1.4 K, are 5.70(6) and 5.49(6) μ_B, respectively. The mean magnetic moment values, calculated from the amplitude $A(k)_i$ with the relation $\mu=A(k)2^{-1/2}$, are 4.03 and 3.88 μ_B for the "k_1" and "k_2" phases, respectively (Table 7).

Neutron diffraction patterns recorded step by step evidence a magnetic ordering below 3 K (Fig. 21). Even if we can observe clearly the growth of the magnetic peaks corresponding to the "k_1" phase before those of the "k_2" phase, it is not possible to determine exactly the temperature of appearance of this later.

6. Discussion

The X-ray and neutron powder diffraction patterns recorded in the paramagnetic state, confirm the CeScSi-type structure for the RMgPb compounds with R=Ce–Nd, Sm, and Gd–Tm. The values refined by neutron powder diffraction are in fair agreement with those encountered in the literature [22].

Macroscopic magnetic measurements performed on the RMgPb compounds evidenced a new series of CeScSi-type structure compounds with antiferromagnetic behaviors. These compounds display magnetic properties (i.e. paramagnetic Curie temperatures, M_{max}, threshold field values) close to those measured for the isostructural RMgSn compounds [2] (Table 2). Moreover, the Néel temperatures determined for the heavy rare-earth RMgPb compounds are similar with those of the RMgSn compounds, suggesting close R–R magnetic interactions. Indeed, it has been shown that R–R contacts play a crucial role in the magnetic interactions in CeScSi- and closely related CeFeSi-type structure compounds [23–25]. Thus, the larger cell parameters of the RMgPb compounds with respect to those of the RMgSn compounds must be compensated by atomic positions adjustment. Like in the RMgSn series [2], the samarium compound presents the higher magnetic ordering temperature, even if the Néel temperature of SmMgPb is lower than that of SmMgSn. This difference of T_N between the RMgPb and RMgSn compounds is also observed for the other light rare-earth compounds.

The temperatures of magnetic ordering deduced from neutron powder experiments are in fair agreement with those determined by macroscopic magnetic measurements. Like for the RMgSn compounds [3], this neutron diffraction study evidences an evolution of the magnetic arrangement of the R moments with the nature of the rare-earth element in the RMgPb series:

(i) CeMgPb is characterized by two propagation vectors, $k_1=[½, ½, 0]$ and $k_2=[0.448, ½, 0]$, which correspond to a commensurate and incommensurate antiferromagnetic structure, respectively. For both, the magnetic moments are located in the (a,b) plane with a ϕ angle of 135°. The magnetic structure corresponding to the propagation vector k_1 is characterized by ferromagnetic [110] chains coupling antiferromagnetically between them in "W" blocks and antiferromagnetically between first neighbors in the "$CeMg_2Si_2$" blocks. A sine-wave modulation of the magnetic moments in the [100] direction is induced by the second propagation vector k_2. This kind of magnetic arrangement has never been observed for CeScSi-type compound.

(ii) PrMgPb and NdMgPb are characterized by a commensurate antiferromagnetic structure with the coupling sequence "++−−" along the [001] direction. The magnetic moment direction deviates from the (001) plane by an angle close to 32° and 33° for PrMgPb and NdMgPb, respectively. Similar magnetic structure has been already observed for PrMgSn and NdMgSn on the whole ordered state [3] and for PrScGe compound between 140 and 82 K [6].

(iii) TbMgPb is characterized by an incommensurate sine-wave modulated magnetic structure from T_N down to 2 K with orientation of the magnetic moments in the (a,b) plane. A thermal evolution is observed for the q_x component and the ϕ angle. At 2 K, the propagation vector is [0.843, 0, 0] and the ϕ angle is close to 42°. Like for TbMgSn [3], the absence of higher order harmonics and the integer total angular momentum of the Tb^{3+} ion ($J=6$), allowing a singlet ground state (non-Kramers ion), indicate that the sine-wave modulated magnetic structure can be stable down to the lower temperatures [26,27].

(iv) DyMgPb, HoMgPb and ErMgPb are characterized by a modulated magnetic structure, which is sine-wave below T_N and squares up at lower temperature in accordance with the occurrence of odd integer harmonics. Thus, at 2 K, DyMgPb

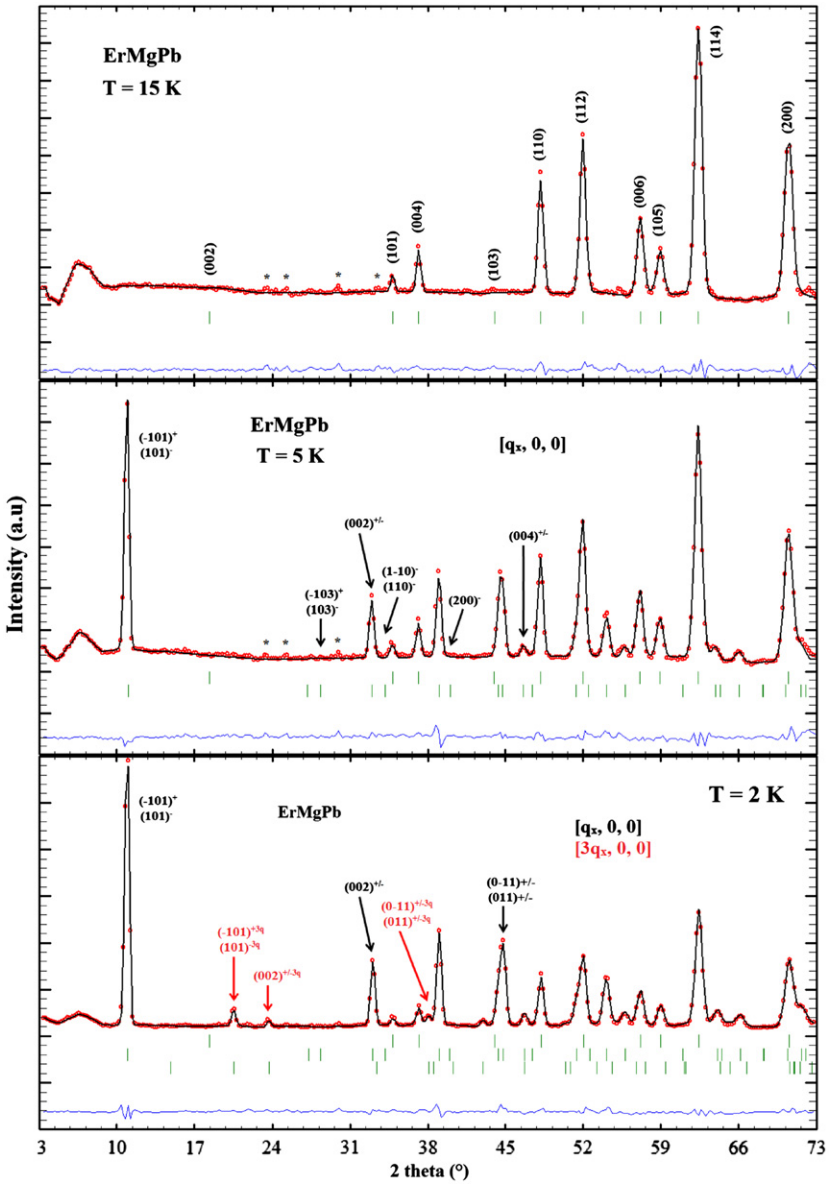

Fig. 17. Observed and calculated neutron diffraction patterns of ErMgPb at 15, 5 and 2 K.

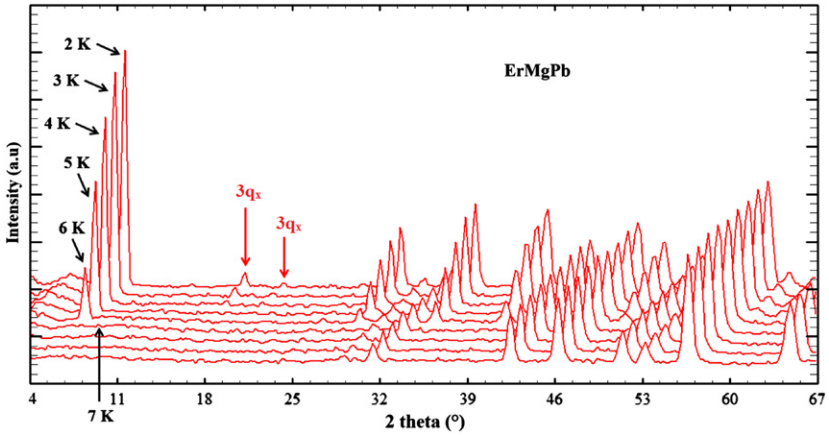

Fig. 18. Observed neutron diffraction patterns of ErMgPb recorded step by step from paramagnetic state down to 2 K.

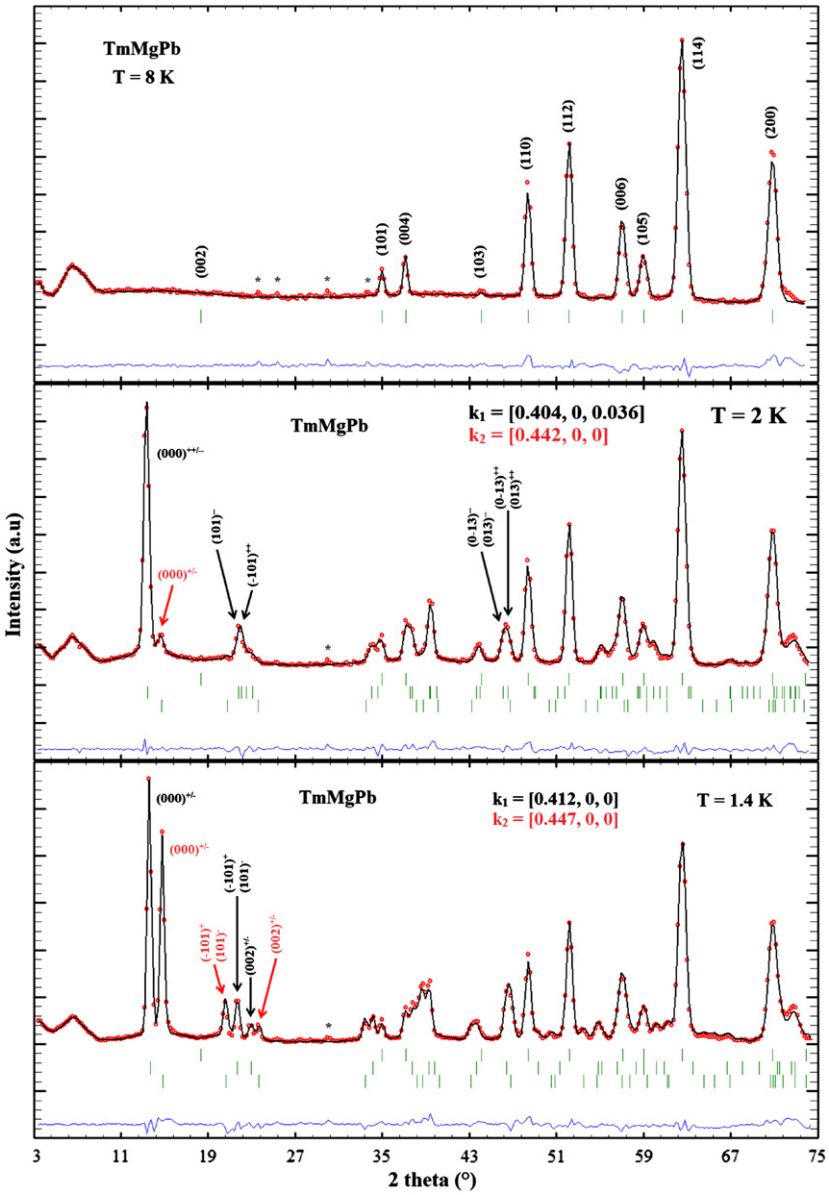

Fig. 19. Observed and calculated neutron diffraction patterns of TmMgPb at 8, 2 and 1.4 K.

and HoMgPb present propagation vectors corresponding to the fundamental, third and fifth harmonics, and ErMgPb presents propagation vectors related to the fundamental and third harmonic. Like for RMgSn (R=Dy, Ho and Er) compounds which present similar magnetic structures [3], HoMgPb and ErMgPb are characterized by only q_x component of the propagation vector, while DyMgPb evidenced q_x and q_y components. Moreover, the magnetic moments of the DyMgPb and HoMgPb compounds are located in the (a,b) plane (like in the corresponding stannides), while those of the ErMgPb are aligned along the c axis (like ErMgSn). A thermal evolution of the q_x component and ϕ angle is observed for HoMgPb, while the important absorption of dysprosium and the low ordering temperature of erbium sublattice do not allow similar behaviors for these compounds.

(v) At 1.4 K, TmMgPb is characterized by the propagation vectors $k_1=[0.412,\ 0,\ 0]$ and $k_2=[0.447,\ 0,\ 0]$, corresponding to incommensurate sine-wave modulated magnetic structures with magnetic moments oriented along the c axis. The slightly different values of q_x components for k_1 and k_2 evidenced by refinements performed between 2 K and 1.4 K, and the q_z component for k_1 refined at 2 K, suggest a thermal evolution of the propagation vectors. Both magnetic structures are characterized by a sine-wave modulation in the [100] direction. This kind of magnetic arrangement has never been observed for CeScSi-type compound.

In the tetragonal CeScSi-type structure, the rare-earth atoms are localized on 4(e) site of *4mm* point symmetry. The rare-earth sublattice easy direction is thus determined by the sign of the second-order crystal field parameter B_2^0 which is given by $B_2^0=\alpha_J r^2(1-\sigma_2)A_2^0$ [28] namely depending simultaneously of α_J and A_2^0. According to Greedan and Rao [28], an easy axis arrangement along the [001] direction indicates a negative B_2^0 term. Since the Stevens factor α_J [29] depends only on the nature of rare-earth atoms, the determining factor is A_2^0.

Neutron diffraction results evidenced a magnetic moments orientation in the (a,b) plane for R=Ce, Tb–Ho and along the c axis for R=Er, Tm. These results are in agreement with the sign of the

second-order Stevens factor α_J. Thus, magnetic moments alignment in the (a,b) plane when R=Ce, Tb, Dy or Ho ($\alpha_J<0$) and along the c axis when R=Er or Tm ($\alpha_J>0$) indicates that the A_2^0 factor must be negative. In this series, the magnetic moments orientation of the R atoms is similar to that determined for the CeScSi-type RMgSn compounds [3] and inverse compared to those of the isotypic compounds, determined by neutron diffraction, $TbTi_{0.85}Mo_{0.15}Ge$ [4], RZrSb (R=Tb–Er) [5] and TbScGe [6], indicating a modification of the electrostatic potential created by environment including transition metal atoms.

Assuming that the sign of A_2^0 remains constant for a same crystallographic site, the negative second-order Stevens factor α_J of Pr and Nd atoms and positive for Sm atom, suggests that the magnetic moment orientation should be in the (a,b) plane for PrMgX and NdMgX (X=Sn, Pb) compounds and along the c axis for SmMgX (X=Sn, Pb) compounds. An easy axis arrangement is effectively suggest by ^{119}Sn Mössbauer spectroscopy for SmMgSn [30] and similar orientation can be extended for SmMgPb compound due to the important magnetic similitude between RMgSn and RMgPb series. Concerning PrMgPb and NdMgPb compounds, the magnetic moment orientation determined by neutron powder diffraction evidenced a deviation from the (a,b) plane, has already observed for the CeScSi-type RMgSn and RScGe (with R=Pr, Nd) compounds [3,6,31,32]. This deviation from the easy plane direction suggests that the second-order crystal field parameter B_2^0 is

Table 7
Refined parameters of TmMgPb compound in the magnetic state.

	2 K	1.4 K
a (Å)	4.347(1)	4.347(1)
c (Å)	15.826(4)	15.824(4)
z_{Tm}	0.335(1)	0.334(1)
z_{Pb}	0.140(1)	0.140(2)
Sine-modulated 1		
θ (deg.)	0	0
$A(k)_{Tm}$	5.83(5)	5.70(6)
q_x	0.404(1)	0.412(1)
q_z	0.036(2)	0
μ_{Tm}[a] (μ_B)	4.12	4.03
Sine-modulated 2		
θ (deg.)	0	0
$A(k)_{Tm}$	1.65(8)	5.49(6)
q_x	0.442(2)	0.447(1)
μ_{Tm}[a] (μ_B)	1.17	3.88
R_{Bragg}; R_f	2.78; 2.38	3.94; 2.80
R_{magn}	8.47; 21.4	8.85; 13.3
R_{wp}; R_{exp}; χ^2	2.50; 0.74; 11.3	3.41; 0.47; 53.7

[a] The mean magnetic moment in the sine-modulated structure μ_i is calculated from the amplitude $A(k)_i$ with the relation $\mu=A(k)2^{-1/2}$.

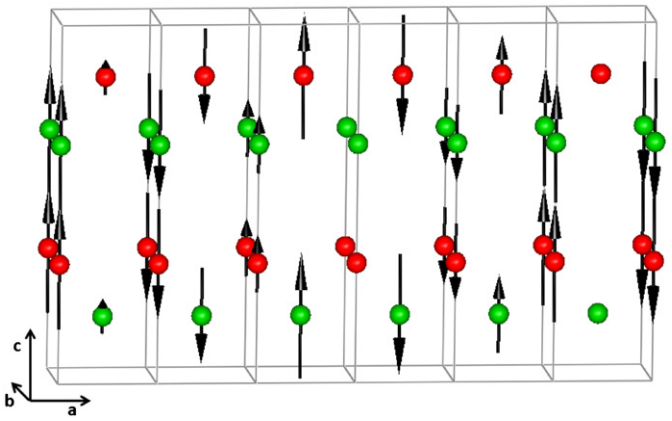

Fig. 20. Magnetic structure corresponding to the propagation vector k_1 of TmMgPb.

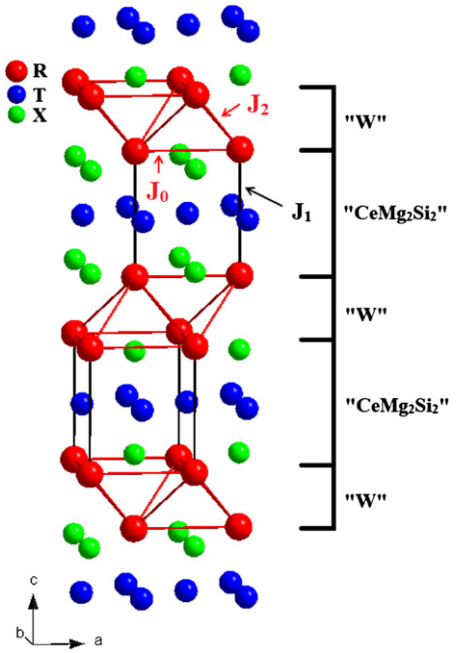

Fig. 22. R–R magnetic interactions in the CeScSi-type structure compounds.

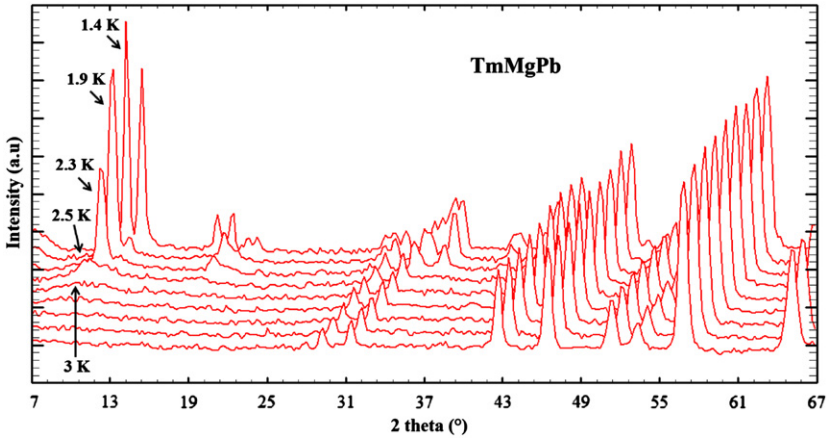

Fig. 21. Observed neutron diffraction patterns of TmMgPb recorded step by step from paramagnetic state down to 1.4 K.

Table 8
Propagation vector and R–R magnetic interactions encountered in the CeScSi-type RMgSn [3] and RMgPb compounds.

RMgSn	Ce	Pr	Nd	Sm	Gd	Tb	Dy	Ho	Er	Tm
q_x	–	0	0	–	–	0.828	0.830	0.822	0.800	0.795
q_y	–	0	0	–	–	0	0.014	0	0	0
q_z	–	1	1	–	–	0	0	0	0	0
J_2	–	F	F	–	–	F+AF	F+AF	F+AF	F+AF	F+AF
J_0	–	F	F	–	–	F+AF	F+AF	F+AF	F+AF	F+AF
J_1	–	AF	AF	–	–	AF	AF	AF	AF	AF
RMgPb	Ce	Pr	Nd	Sm	Gd	Tb	Dy	Ho	Er	Tm
q_x	0.5	0	0	–	–	0.843	0.841	0.835	0.816	0.412; 0.447
q_y	0.5	0	0	–	–	0	0.016	0	0	0; 0
q_z	0	1	1	–	–	0	0	0	0	0; 0
J_2	F+AF	F	F	–	–	F+AF	F+AF	F+AF	F+AF	F+AF
J_0	AF	F	F	–	–	F+AF	F+AF	F+AF	F+AF	F+AF
J_1	AF	AF	AF	–	–	AF	AF	AF	AF	F

not preponderant and influence of crystal field terms of rank higher than two is expected [33,34].

The modulated magnetic structure evidenced for the RMgPb compounds supported the metamagnetic-like behaviors observed by macroscopic magnetic measurements on a large range of applied magnetic field and the paramagnetic Curie temperatures close to 0 K. Indeed, these rather complicated magnetic structures suggest a competition between opposite magnetic interactions.

These magnetic arrangements are dependent on magnetic interactions (Fig. 22) generated by the lanthanide atoms located on either side of the T square planes (J_1) and inside the (R,X) slabs (J_0 and J_2). The CeScSi-type RMgPb and RMgSn compounds are characterized by antiferromagnetic J_1 interactions in the "$CeMg_2Si_2$" blocks (Table 8), according to the opposite magnetic phase angle between the two rare-earth "sublattices" (Fig. 4), excepted for TmMgPb which presents ferromagnetic J_1 interactions in the "$CeMg_2Si_2$" blocks (Table 8). The RMgX (X=Sn, Pb) compounds with heavy rare-earth are characterized by competition between both ferro- and antiferromagnetic J_0 and J_2 interactions in the "W" blocks due to their modulated magnetic structures, while the CeScSi-type PrMgX and NdMgX (with X=Sn, Pb) evidences only ferromagnetic J_0 and J_2 interactions (commensurate antiferromagnetic structure) and CeMgPb antiferromagnetic J_0 interactions and competition between ferromagnetic and antiferromagnetic J_2 interactions in the "W" blocks (Table 8).

7. Conclusion

The RMgPb (with R=Ce–Nd, Sm, Gd–Tm) compounds crystallize in the CeScSi-type structure in agreement with the crystallographic data published by Provino et al. [7]. Like for the RMgSn compounds [2], macroscopic magnetic measurements evidenced antiferromagnetic behaviors for all the CeScSi-type RMgPb compounds, while the most other ternary CeScSi-type compounds are ferromagnets.

The neutron powder diffraction study of the RMgPb series evidences similar magnetic structures for R=Pr, Nd, Tb, Dy, Ho and Er atoms with those of the RMgSn compounds [3]. In these series, we observed commensurate antiferromagnetic structures for R=Pr and Nd, incommensurate sine-wave modulated magnetic structure for R=Tb down to 2 K and commensurate or incommensurate modulated magnetic structures which are sine-wave below T_N and tend to be square up at very low temperature for R=Dy, Ho and Er.

On contrary, the magnetic structures are different for R=Ce, due to different crystallographic structures (TiNiSi- and CeScSi-type for CeMgSn and CeMgPb, respectively), and for R=Tm. Indeed, at lower temperature, TmMgSn evidences a magnetic structure similar to those observed with R=Dy, Ho and Er compounds, characterized by propagation vectors [q_x, 0, 0] and [$3q_x$, 0, 0] while TmMgPb evidences two propagation vectors [q_x, 0, 0] without appearance of higher order harmonics.

These two series present the same magnetic moments orientation of the R atoms, which is inverse compare to the other CeScSi-type structure compounds. The magnetic moments deviation from the (a,b) plane observed for PrMgX and NdMgX (X=Sn, Pb) suggests influence of crystal field terms of rank higher than two.

These complex magnetic structures are due to competitions between ferromagnetic and antiferromagnetic interactions, which depend of the nature of the rare-earths element. In order to better understand the magnetic interactions encountered in the CeScSi-type structure compounds, it will be now very interesting to study the solid solution $TmMgSn_{1-x}Pb_x$ to check evolution from ferromagnetic (TmMgPb) to antiferromagnetic (TmMgSn) J_1 interactions in the "$CeMg_2Si_2$" blocks.

Acknowledgments

The authors are indebted to the Institut Laue Langevin (Grenoble, France) for the provision of research facilities (proposal 5-31-2062).

References

[1] P. Manfrinetti, A. Provino, K.A. Gschneidner Jr., Journal of Alloys and Compounds 482 (2009) 81.
[2] P. Lemoine, A. Vernière, J.F. Marêché, B. Malaman, Journal of Alloys and Compounds 508 (2010) 9.
[3] P. Lemoine, A. Vernière, G. Venturini, S. Capelli, B. Malaman, Journal of Magnetism and Magnetic Materials 324 (2012) 961.
[4] A.V. Morozkin, A.I. Kurbakov, V. Klosek, R. Welter, Journal of Alloys and Compounds 315 (2001) 100.
[5] A.V. Morozkin, K. Halich, R. Welter, B. Ouladdiaf, Journal of Alloys and Compounds 393 (2005) 34.
[6] P. Manfrinetti, A.V. Morozkin, O. Isnard, P. Henry, A. Palenzona, Journal of Alloys and Compounds 450 (2008) 86.
[7] A. Provino, K.A. Gschneidner Jr., P. Manfrinetti, Journal of Alloys and Compounds 497 (2010) 131.
[8] J. Rodriguez-Carvajal, Physica B 192 (1993) 55.
[9] T. Roisnel, J. Rodriguez-Carvajal, Materials Science Forum 378–381 (2001) 118.
[10] P.G. de Gennes, Journal de Physique et le Radium 23 (1962) 510.
[11] M.A. Ruderman, C. Kittel, Physical Review 96 (1954) 99.
[12] T. Kasuya, Progress Of Theoretical Physics (Kyoto) 16 (1956) 45.
[13] K. Yosida, Physical Review 106 (1957) 893.
[14] S. Baran, M. Hofmann, J. Leciejewicz, M. Slaski, A. Szytula, A. Zygmunt, Journal of Physics: Condensed Matter 9 (1997) 9053.
[15] R. Welter, A. Vernière, G. Venturini, B. Malaman, Journal of Alloys and Compounds 283 (1999) 54.
[16] W. Hermes, R. Pöttgen, Solid State Sciences 11 (2009) 706.

[17] E. Belorizky, J.J. Niez, P.M. Levy, Physical Review B 23 (1981) 3360.
[18] J. Rossat-Mignod, Methods of Experimental Physics C23 (1987) 121 (Academic Press. Inc.).
[19] B. Malaman, G. Venturini, A. Blaise, J.P. Sanchez, G. Amoretti, Physical Review B 47 (1993) 8681.
[20] A. Blaise, B. Fak, J.P. Sanchez, G. Amoretti, P. Santini, R. Caciuffo, D. Schmitt, B. Malaman, G. Venturini, Journal of Physics: Condensed Matter 7 (1995) 8317.
[21] P. Schobinger-Papamantellos, M. Kenzelmann, A. Schenck, F.N. Gygax, K.H.J. Buschow, C. Ritter, Physica B: Condensed Matter 349 (2004) 100.
[22] P. Villars, K. Cenzual, Pearson's Crystal Data—Crystal Structure Database for Inorganic Compounds, Release 2010/11, ASM International, Materials Park, Ohio, USA.
[23] V. Klosek, A. Vernière, B. Ouladdiaf, B. Malaman, Journal of Magnetism and Magnetic Materials 246 (2002) 233.
[24] R. Welter, A.V. Morozkin, K. Halich, Journal of Magnetism and Magnetic Materials 257 (2003) 44.
[25] S. Couillaud, E. Gaudin, V. Franco, A. Conde, R. Pöttgen, B. Heying, U.Ch. Rodewald, B. Chevalier, Intermetallics 19 (2011) 1573.
[26] J. Rossat-Mignod, Methods of Experimental Physics C23 (1987) 132. (Academic Press. Inc.).
[27] D. Gignoux, D. Schmitt, Journal of Alloys and Compounds 326 (2001) 143.
[28] J.E. Greedan, C.N. Rao, Journal of Solid State Chemistry 6 (1973) 387.
[29] K.W.H. Stevens, Proceedings of the Physical Society (London) A65 (1952) 209.
[30] G. Le Caër, Private communication.
[31] J.M. Cadogan, D.H. Ryan, R. Gagnon, C.J. Voyer, Journal of Applied Physics 97 (2005) 10A916.
[32] J.M. Cadogan, D.H. Ryan, Solid State Phenomena 170 (2011) 282.
[33] B.K. Cho, P.C. Canfield, L.L. Miller, D.C. Johnston, W.P. Beyermann, A. Yatskar, Physical Review B 52 (1995) 3684.
[34] A. Vernière, V. Klosek, R. Welter, G. Venturini, O. Isnard, B. Malaman, Journal of Magnetism and Magnetic Materials 234 (2001) 261.